DOI 10.1007/s11223-021-00316-9
*Strength of Materials, Vol. 53, No. 4, July, 2021*

# CONSTRUCTION OF THE THEORY OF PLASTICITY IRRELATIVE OF THE LOADING SURFACE AND ASSOCIATED FLOW LAW

**V. S. Bondar,[1] D. R. Abashev, and V. K. Petrov**

UDC 539.374

*The experimental uniaxial cyclic loading diagram for a 40Kh16N9G2S steel specimen was analyzed to define the three sections representing different stress behavior, i.e., three different stress modes. For each stress mode, the corresponding evolutionary equations governing anisotropic hardening were formulated. For describing the isotropic hardening, the evolutionary equation for the second-mode saturation parameter is introduced. The stress deviator is defined as the sum of stress deviators of the three modes. The nonlinear damage accumulation is represented by the kinetic equation based on the energy principle, where the energy equal to the work of second-mode stresses within the strain field is taken as the energy spent for damaging of the material. The material functions governing the theory are defined, the basic experiment and the identification method of the material functions are formulated. The material functions of 40Kh16N9G2S steel and theory verification results under proportional strain-controlled cyclic loading and nonproportional loading along the strain path in the form of concentric circles with the common center in the origin of coordinates are presented. Five path turns are examined, starting from the large-curvature path to the mean-curvature one. Computational and experimental results are in close agreement.*

***Keywords***: plasticity, cyclic loading diagram, loading surface, damage accumulation, material functions, identification, verification.

**Introduction.** Mathematical simulation of deformation processes under arbitrary nonproportional cyclic loading is mainly based on the plastic flow theory versions under multicomponent hardening, which are reviewed and analyzed in [1–13]. The main problem in constructing those versions is the formulation of sufficiently adequate evolutionary equations for the displacement of the loading surface center, as well as the ambiguity of the experimental determination of the loading surface boundaries. In the flow theory, elastic and plastic strains are distinguished. The loading surface-associated flow law (gradient flow law) is used to determine plastic strains.

The present study, making use of experimental results under cyclic loading, viz cyclic hysteresis loops (cyclic loading diagrams), defines three stress modes, with formulating corresponding evolutionary equations. Those three stress modes are consistent with anisotropic hardening. For its description, the evolutionary equation for the second-mode stress saturation parameter is introduced. The combined stress deviator is defined as the sum of the three stress deviators.

The kinetic equation, is set up to describe nonlinear damage accumulation, processes similarly to [1–4, 14–16], where the energy equal to the work of second-mode stresses in the total strain field is taken as the energy spent for damaging the material.

The proposed plasticity theory version features strain as an integral value without distinguishing between elastic and plastic ones, as well as the loading surface concept and, accordingly, the associated flow law is not used.

Moscow Polytechnic University, Moscow, Russia ([1]v.s.bondar@mospolytech.ru). Translated from Problemy Prochnosti, No. 4, pp. 28 – 36, July – August, 2021. Original article submitted August 11, 2020.

 

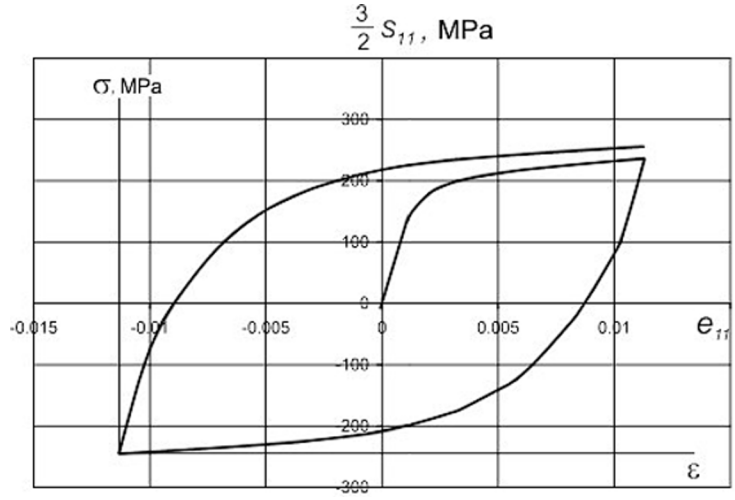


Fig. 1. Hysteresis loop.

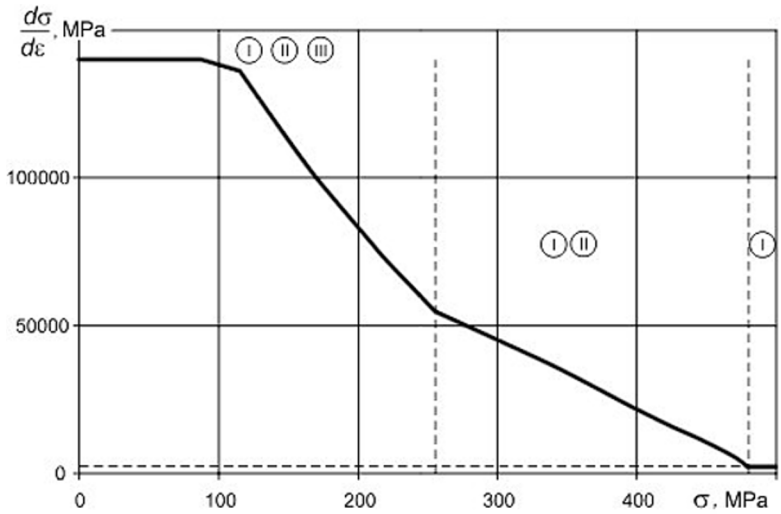


Fig. 2. Curve in the $d\sigma/d\varepsilon - \sigma$ coordinates.

The material functions that govern the theory version and are subject to experimental determination are defined. The basic experiment and identification method of material functions are formulated. Experimental material functions of 40Kh16N9G2S steel are presented [17, 18]. The theory is verified under proportional and nonproportional cyclic loading.

**1. Basic Theory Concepts and Equations.** The hysteresis loop (Fig. 1) is examined in the deviator components $\frac{3}{2}s_{11}$ and $e_{11}$ in uniaxial tension–compression to derive the plasticity theory relations. Then, on the half-cycle from the deformation direction change point, the coordinate stress $\sigma$ – strain $\varepsilon$ system is introduced. The curve in the $\sigma, \varepsilon$ coordinates includes elastic and plastic strains without distinguishing between them. Then, the $d\sigma/d\varepsilon$ derivative is calculated and the curve is plotted in the $d\sigma/d\varepsilon$ and $\sigma$ coordinates (Fig. 2).

On this curve, the three sections characterizing different stress behavior can be defined. On the first section ($\sigma > 480$ MPa), the derivative is practically constant, and here the evolutionary equation similar to the Ishlinskii–Prager one [19, 20] for first-mode microstresses [15, 16] is proposed for the first-mode stresses

$$\dot{s}_{ij}^{(1)} = \frac{2}{3} g^{(1)} \dot{e}_{ij}. \tag{1}$$

In the second section $\{\sigma \in (250, 480]$ MPa$\}$, the derivative varies linearly, and the evolutionary equation, similar to the Amstrong–Frederick–Kadashevich one [21, 22] for second-mode microstresses [15, 16], is proposed for the second-mode stresses

$$\dot{s}_{ij}^{(2)} = \frac{2}{3} g^{(2)} \dot{e}_{ij} + g_s^{(2)} s_{ij}^{(2)} \dot{\varepsilon}_{u*} \qquad \left( \dot{\varepsilon}_{u*} = \left( \frac{2}{3} \dot{e}_{ij} \dot{e}_{ij} \right)^{1/2} \right). \tag{2}$$

Then, in the third section $(\sigma \in [0, 250]$ MPa$)$, the derivative varies nonlinearly, which can be described by a set of evolutionary equations of the Ohno–Wang type [3, 23] for the third-mode microstresses [15, 16]

$$\dot{s}_{ij}^{(m)} = \frac{2}{3} g^{(m)} \dot{e}_{ij} \qquad (m = 3, \ldots, M). \tag{3}$$

The defining functions $g^{(1)}$, $g^{(2)}$, $g_s^{(2)}$, $g^{(m)}$ in Eqs. (1)–(3), are expressed [1–3, 14–16] via the material ones as follows:

$$g^{(1)} = E_{s0}, \qquad g^{(2)} = \beta \sigma_{s0}, \qquad g_s^{(2)} = -\beta, \tag{4}$$

$$g^{(m)} = \begin{cases} \beta^{(m)} \sigma_s^{(m)}, \\ 0, \quad \text{if} \quad \sigma_u^{(m)} \ge \sigma_s^{(m)} \bigcap s_{ij}^{(m)} \dot{e}_{ij} > 0, \end{cases} \tag{5}$$

$$\left( \sigma_u^{(m)} = \left( \frac{3}{2} s_{ij}^{(m)} s_{ij}^{(m)} \right)^{1/2}, \quad m = 3, \ldots, M \right).$$

Isotropic hardening and softening are described with the relation between the saturation parameter $\sigma_s$ for the second-mode stress and the accumulated strain $\varepsilon_{u*}$

$$\sigma_{s0} = \sigma_{s0}(\varepsilon_{u*}) \quad (\varepsilon_{u*} = \int \dot{\varepsilon}_{u*} dt). \tag{6}$$

Here in Eqs. (4)–(6), $E_{s0}$, $\sigma_{s0}(\varepsilon_{u*})$, $\beta$, $\sigma_s^{(m)}$, and $\beta^{(m)}$ are the material functions subject to experimental determination.

The stress deviator similar to the Novozhilov–Chaboche model [24, 25] for microstresses [15, 16] is defined as the sum of three-mode stresses with the corresponding evolutionary equation:

$$s_{ij} = \sum_{m=1}^{M} s_{ij}^{(m)}. \tag{7}$$

The equation for the stress deviator in view of (1)–(3) and (7), would finally have the following form:

$$\dot{s}_{ij} = \frac{2}{3} g \dot{e}_{ij} + g_s^{(2)} s_{ij}^{(2)} \dot{\varepsilon}_{u*}, \tag{8}$$

$$g = \sum_{m=1}^{M} g^{(m)}. \tag{9}$$

The equation relating the spherical components of the stress $\sigma_0 = \sigma_u / 3$ and strain $\varepsilon_0 = \varepsilon_u / 3$ tensors: should be added to Eq. (8)

$$\sigma_0 = 3K\varepsilon_0. \tag{10}$$

For describing the nonlinear processes of damage accumulation, the kinetic equation is introduced based on the energy principle, where the energy equal to the work of second-mode stresses in the strain field is taken as the energy spent for damaging the material. This kinetic equation is introduced by analogy with the kinetic one [15, 16] based on the work of second-mode microstresses in the plastic strain field. Then the kinetic equation of damage accumulation will have the following form:

$$\dot{\omega} = \alpha\omega^{(\alpha-1)/\alpha}\,\frac{s_{ij}^{(2)}\dot{e}_{ij}}{W_{s0}}, \tag{11}$$

$$\alpha = (\sigma_{s0}/\sigma_u^{(2)})^{n_\alpha}. \tag{12}$$

Here $\omega$ is the damage measure, $W_{s0}$ is the fracture energy, $\alpha$ and $n_\alpha$ are the function and parameter of the damage accumulation nonlinearity ($n_\alpha = 1.5$ practically for all structural steels and alloys), and $\sigma_u^{(2)}$ is the second-mode stress intensity.

The version of the plasticity theory, in contrast to the versions of the plastic flow theory, has the following features:

(i) elastic and plastic strains are not distinguished;

(ii) introduction of the loading (yield) surface is not necessary;

(iii) associated flow law is not used;

(iv) introduction of loading or unloading conditions (elastic or elastoplastic conditions) is not necessary;

(v) second-mode stresses are calculated that coincide with second-mode microstresses responsible for the damage accumulation process.

Thus, this version of the plasticity theory is governed with the following material functions subject to experimental determination: $K$ and $G$ are the volumetric elasticity and shear moduli, $E_{s0}$, $\sigma_{s0}(\varepsilon_{u*})$, $\beta$, $\sigma_s^{(m)}$, $\beta^{(m)}$ ($m = 3, \ldots, M$) are the anisotropic hardening moduli, and $W_{s0}$ is the fracture energy.

**2. Computation-Experimental Method of Determining the Material Functions.** The material functions are determined from the test results in a uniaxial stress state (tension–compression or torsion). The basic experiment includes the following data set:

(i) volumetric elasticity and shear moduli determined by conventional methods;

(ii) tensile (torsion) diagram to the strain of 0.05–0.1;

(iii) cyclic loading diagram in symmetrical tension–compression or alternating torsion at a constant strain range of 0.02–0.03;

(iv) data on low-cycle fatigue under strain-controlled symmetrical cyclic loading.

Here and hereafter, strain-controlled loading corresponds to that at preset strains.

For determining the anisotropic hardening moduli, the hysteresis loop (cyclic diagram) is reconstructed in the stress $\sigma$ – strain $\varepsilon$ coordinates (Fig. 1). The origin of this coordinate system is located in the deformation direction change point.

Then the $d\sigma/d\varepsilon$ derivative is calculated, and the curve is plotted in the $d\sigma/d\varepsilon - \sigma$ coordinates (Fig. 2). On the curve (Fig. 2) the three sections characterizing different behavior of the $d\sigma/d\varepsilon$ derivative are defined. On the first section, the derivative is practically constant, equal to the parameter $E_{s0}$. Then the curve in Fig. 2 is reconstructed in the coordinates:

$$d\hat{\sigma}/d\varepsilon = (d\sigma/d\varepsilon - E_{s0}) \qquad \text{and} \qquad \hat{\sigma} = (\sigma - E_{s0}\varepsilon),$$

i.e., the effect of first-mode stresses is excluded. The linear relation on the second section (Fig. 3) is used to find the parameters $\sigma_{s0}$ and $\beta$ by the following formulas:

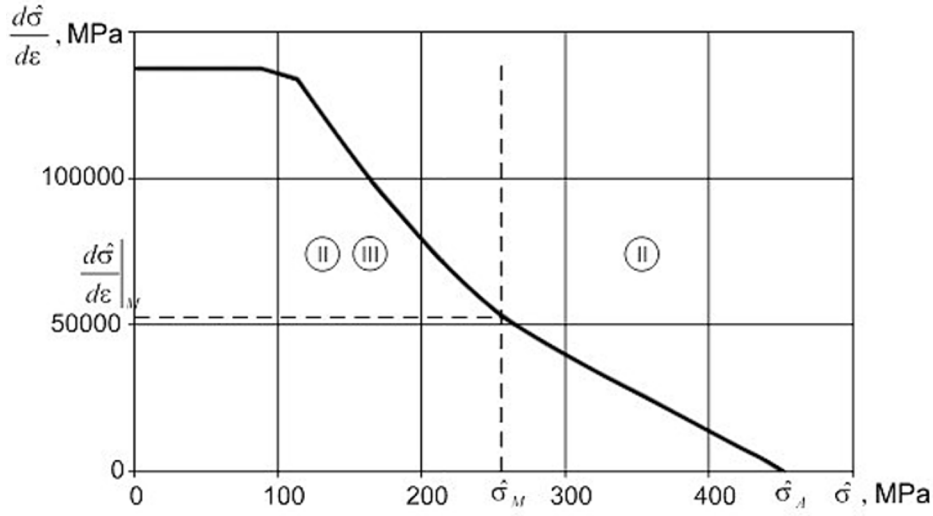


Fig. 3. Curve in the $d\hat{\sigma}/d\varepsilon - \hat{\sigma}$ coordinates.

$$\beta = \left.\frac{d\hat{\sigma}}{d\varepsilon}\right|_M \Big/ (\hat{\sigma}_A - \hat{\sigma}_M), \tag{13}$$

$$\sigma_{s0} = \frac{\hat{\sigma}_A - \hat{\sigma}_M}{2\exp(-\beta\varepsilon_M)}. \tag{14}$$

Here $\varepsilon_M$ is the strain of the third section end (end of the third-mode) stress change.

The curve in Fig. 1 is then rebuilt in the coordinates:

$$\tilde{\sigma} = \sigma - E_{s0}\varepsilon - 2\sigma_{s0}[1 - \exp(-\beta\varepsilon)] \quad \text{and} \quad \varepsilon \quad (\varepsilon \in [0, \varepsilon_M]).$$

The curve (Fig. 4) corresponds to the third-mode stresses only. The length of the third section is quite small $\varepsilon_M \approx 0.002$–$0.004$, i.e., the third-mode stresses practically arise within the operating residual strain tolerance in determining the yield limit. Then the interval $[0; \tilde{\sigma}_M]$ is divided into the $(M-2)$ parts, and the anisotropic hardening parameters are calculated by the following formulae:

$$\beta^{(m)} = 2/\varepsilon_m \qquad (m = 3, \ldots, M), \tag{15}$$

$$\sigma_s^{(M)} = \frac{\tilde{\sigma}_M - \tilde{\sigma}_{M-1}}{\varepsilon_M - \varepsilon_{M-1}} \frac{1}{\beta^{(M)}}, \tag{16}$$

$$\sigma_s^{(m)} = \frac{1}{\beta^{(m)}} \left[ \frac{\tilde{\sigma}_m - \tilde{\sigma}_{m-1}}{\varepsilon_m - \varepsilon_{m-1}} - \frac{\tilde{\sigma}_{m+1} - \tilde{\sigma}_m}{\varepsilon_{m+1} - \varepsilon_m} \right] \qquad (m = M-1, \ldots, 3; \tilde{\sigma}_2 = 0; \varepsilon_2 = 0). \tag{17}$$

With the anisotropic hardening parameters, the isotropic hardening level can be calculated. For this, the experimental tension diagram and experimental stress values at the end of tension half-cycles are used. By fitting the calculated stress values at the corresponding accumulated strains until their coincidence with the experimental stress values, the isotropic hardening function $\sigma_{s0}(\varepsilon_{u*})$ can be obtained. The initial $\sigma_{s0}(0)$ value is determined by the following formula:

$$\sigma_{s0}(0) = \frac{1}{\beta}\left( 3G - E_{s0} - \sum_{m=3}^{M} \beta^{(m)} \sigma_s^{(m)} \right). \tag{18}$$

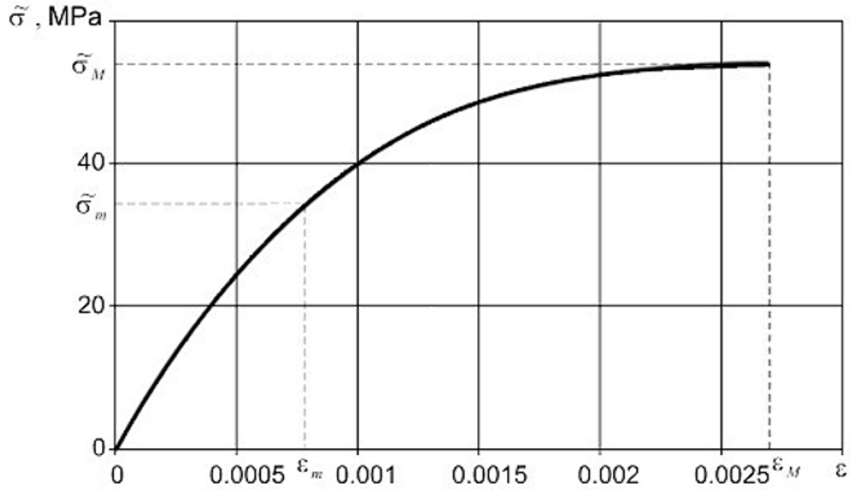


Fig. 4. Curve in the $\tilde{\sigma} - \varepsilon$ coordinates.

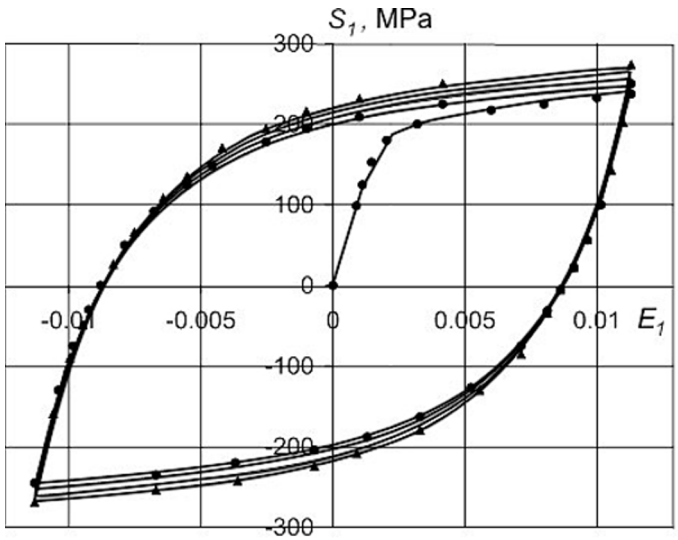


Fig. 5. Cyclic diagrams.

Here $G$ is the shear modulus. Then, the iterative match of $\sigma_{s0}(\varepsilon_{u*})$ values is made for growing accumulated strains.

The fracture energy $W_{s0}$ is evaluated by calculating the second-mode stress work under cyclic loading to the experimental values of the number of cycles to fracture.

The material functions of 40Kh16N9G2S steel obtained in the experiment [17, 18] are given below.

Here, the deformation curve at the first half-cycle of cyclic loading (Fig. 5) and the tension diagram of this steel [17, 18] are used to obtain the material functions.

$$E_{s0} = 3600 \text{ MPa}, \ \beta = 320.$$

| $\varepsilon_{u*}$ | 0 | 0.0016 | 0.0024 | 0.0033 | 0.0092 | 0.028 | 0.046 | 0.083 | 0.122 | 0.25 |
|---|---|---|---|---|---|---|---|---|---|---|
| $\sigma_{s0}$, MPa | 484 | 400 | 202 | 233 | 233 | 236 | 239 | 251 | 261 | 287 |

$$\beta^{(3)} = 3060, \ \sigma_s^{(3)} = 12.2 \text{ MPa}, \ \beta^{(4)} = 1530, \ \sigma_s^{(4)} = 11.8 \text{ MPa}, \ \beta^{(5)} = 905, \ \sigma_s^{(5)} = 9.1 \text{ MPa}.$$

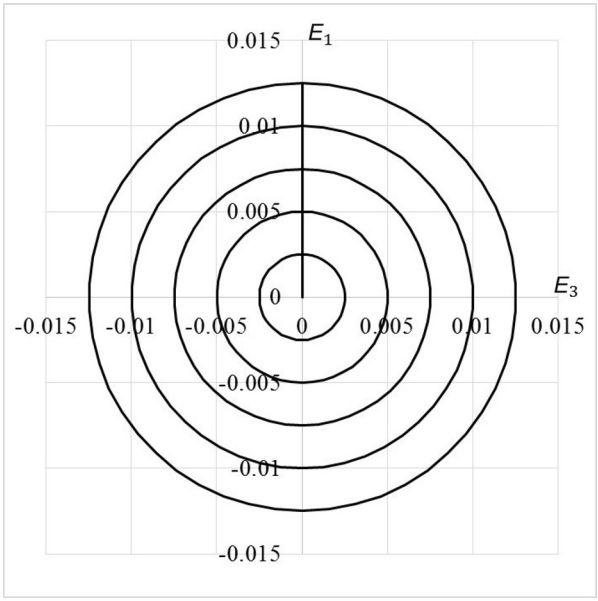


Fig. 6. Path of strains.

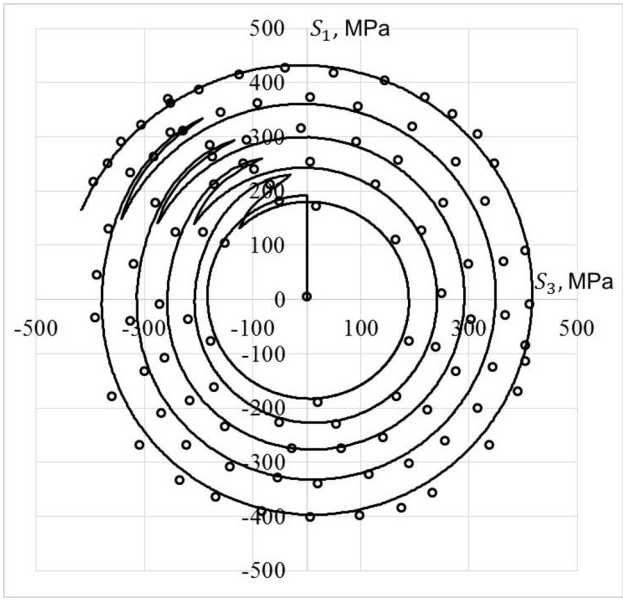


Fig. 7. Path of stresses.

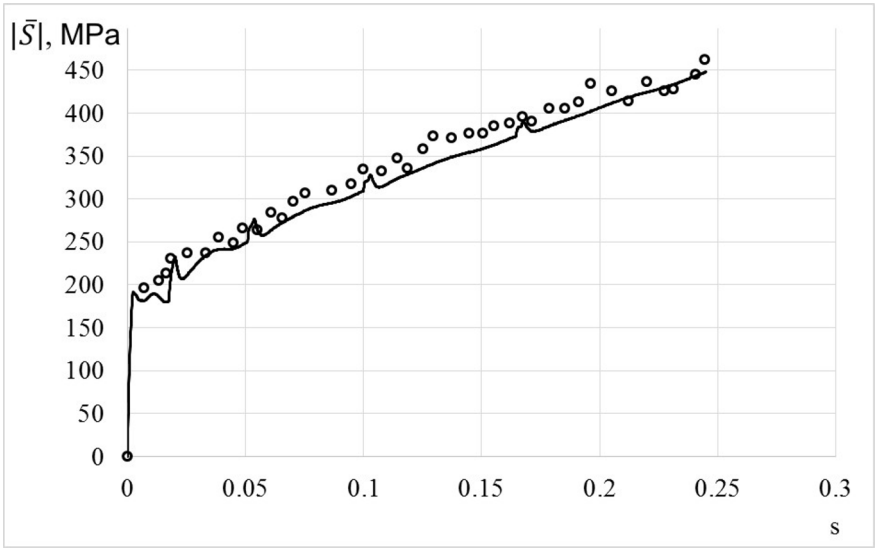


Fig. 8. Scalar properties.

**3. Plastic Deformation under Proportional and Nonproportional Cyclic Loadings.** The theoretical experiment and comparison with the results of experimental studies are carried out on 40Kh16N9G2S steel under proportional and nonproportional cyclic loading. The calculated cyclic diagram for strain-controlled symmetrical uniaxial loading with the strain range $\Delta E_1 = 0.0226$ is shown in Fig. 5. The four loading cycles were performed. Calculation results are presented with the solid curve, experimental results [17, 18] are designated with dark circles (zero and first cycles) and dark triangles (fourth cycle). Hereinafter, the calculated and experimental results are given in the Ilyushin vector representation of strains and stresses [26].

Calculated and experimental [17, 18] results for nonproportional loading of 40Kh16N9G2S steel along the strain path (Fig. 6) in the form of concentric circles with the common center, coinciding with the origin of coordinates, are presented in Figs. 6–9. The transition from one circle to another is performed along the rectilinear path coinciding with the radius. The total of five path turns with the radii of curvature of 0.0025, 0.005, 0.0075, 0.01, and 0.0125 are realized. The transition to each subsequent turn is carried out as a result of additional loading by $E_i$.

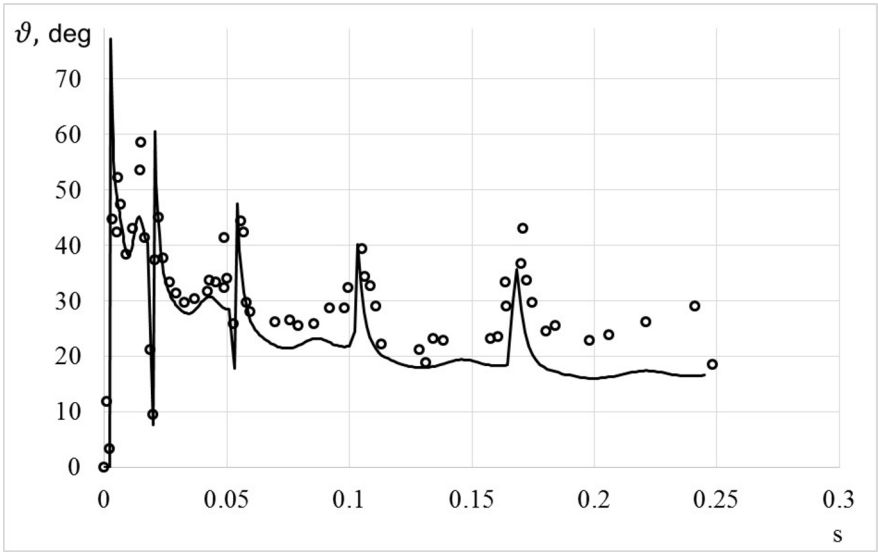


Fig. 9. Vector properties.

The calculated path of stresses is shown with solid curves and the experimental ones [17, 18] are designated with open circles (Fig. 7). The scalar and vector properties (changes in the stress vector length and the angle of deflection of the stress vector from the tangent to the strain path are presented in Figs. 8 and 9, respectively (solid curves are the calculation, open circles are the experiment [17, 18]). The calculated and experimental results for proportional and nonproportional cycle loading display satisfactory agreement.

**Conclusions.** The basic principles and equations of the version of the theory of plasticity without distinguishing between elastic and plastic strains and introducing the loading surface and the associated flow law were formulated.

The formulation of the kinetic equation for nonlinear damage accumulation processes is based on the fact that the work of second-mode stresses in the field of total strains, as well as the work of second-mode microstresses in the field of plastic strains, is the universal characteristic of the material fracture at cyclic loads. The material functions that govern the theory are defined, and a fairly simple basic experiment and method for identifying the material functions are formulated.

The results of calculations and experiments under proportional and nonproportional cyclic loading of 40Kh16N9G2S steel are compared. The strain paths from large to mean curvatures were examined. The above results exhibit satisfactory agreement, which is indicative of adequate efficiency of the proposed version of the theory of plasticity.

## REFERENCES

1. V. S. Bondar, *Inelasticity. Variants of the Theory* [in Russian], Fizmatlit, Moscow (2004).
2. V. S. Bondar and V. V. Danshin, *Plasticity. Proportional and Nonproportional Loads* [in Russian], Fizmatlit, Moscow (2008).
3. V. S. Bondar, *Inelasticity. Variants of the Theory*, Begell House, New York (2013).
4. L. A. Volkov and Yu. G. Korotkikh, *Equations of State of Visco-Elastoplastic Damaged Media* [in Russian], Fizmatlit, Moscow (2008).
5. S. Bari and T. Hassan, "An advancement in cyclic plasticity modeling for multiaxial ratcheting simulation," *Int. J. Plasticity*, **18**, 873–894 (2002).
6. G. Kang, Y. Liu, J. Ding, and Q. Gao, "Uniaxial ratcheting and fatigue failure of tempered 42CrMo steel: Damage evolution and damage-coupled viscoplastic constitutive model," *Int. J. Plasticity*, **25**, 838–860 (2009).

7. Q. Kan and G. Kang, "Constitutive model for uniaxial transformation ratcheting of super-elastic NiTi shape memory alloy at room temperature," *Int. J. Plasticity*, **26**, 441–465 (2010), https://doi.org/10.1016/j.ijplas.2009.08.005.
8. J.-L. Chaboche, "A review of some plasticity and viscoplasticity constitutive theories," *Int. J. Plasticity*, **24**, 1642–1692 (2008).
9. S. M. Rahman, T. Hassan, and E. Corona, "Evaluation of cyclic plasticity models in ratcheting simulation of straight pipes under cyclic bending and steady internal pressure," *Int. J. Plasticity*, **24**, 1756–1791 (2008).
10. M. Abdel-Karim, "Modified kinematic hardening rules for simulations of ratcheting," *Int. J. Plasticity*, **25**, 1560–1587 (2009).
11. M. Abel-Karim, "An evaluation for several kinematic hardening rules on prediction of multiaxial stress-controlled ratcheting," *Int. J. Plasticity*, **26**, 711–730 (2010).
12. Y. F. Dafalias and H. P. Feigenbaum, "Biaxial ratcheting with novel variations of kinematic hardening," *Int. J. Plasticity*, **27**, 479–491 (2011).
13. J.-L. Chaboche, P. Kanouté, and F. Azzouz, "Cyclic inelastic constitutive equations and their impact on the fatigue life predictions," *Int. J. Plasticity*, **35**, 44–66 (2012).
14. V. S. Bondar, S. V. Burchakov, and V. V. Danshin, "Mathematical modeling of elastoplastic deformation and fracture of materials under cyclic loading," in: *Problems of Strength and Plasticity* [in Russian], Interuniversity Proceedings, Vol. 72, Publishing House of Nizhny Novgorod State University, Nizhny Novgorod (2010), pp. 18–27.
15. V. S. Bondar, V. V. Danshin, and D. A. Makarov, "Mathematical modeling of deformation and damage accumulation processes under cyclic loading," *Vestn. PNIPU. Mekhanika*, No. 2, 125–152 (2014).
16. V. S. Bondar, V. V. Dansin, D. Yu. Long, and D. D. Nguyen, "Constitutive modeling of cyclic plasticity deformation and low-high-cycle fatigue of stainless steel 304 in uniaxial stress state," *Mech. Adv. Mater. Struct.*, **25**, No. 12, 1009–1017 (2018), https://doi.org/10.1080/15376494.2017.1342882.
17. N. L. Okhlopkov, *Elastoplastic Deformation Mechanisms of Metals at the Multiaxial Stress State and Nonproportional Loading* [in Russian], Author's Abstract of the Doctor Degree Thesis (Tech. Sci.), Tver TSTU (1997).
18. V. T. Zubchaninov, N. L. Okhlopkov, and V. V. Garannikov, *Experimental Plasticity* [in Russian], Book 1: *Processes of Nonproportional Deformation*, TGTU, Tver (2003).
19. A. Yu. Ishlinskii, "General theory of plasticity with linear hardening," *Ukr. Math. Zhurn*., **6**, Issue 3, 314–324 (1954).
20. W. Prager, "The theory of plasticity: A survey of recent achievements," *P. I. Mech. Eng.*, **169**, 41–57 (1955), https://doi.org/10.1243/PIME_PROC_1955_169_015_02.
21. P. J. Amstrong and C. O. Frederick, *A Mathematical Representation of the Multiaxial Bauschinger Effect*, CEGB Report No. RD/B/N/731 (1966).
22. Yu. I. Kadashevich, "Different tensor-linear relations in the theory of plasticity," in: *Studies on Elasticity and Plasticity* [in Russian], Vol. 6, LGU, Leningrad (1967), pp. 39–45.
23. N. Ohno and J.-D. Wang, "Kinematic hardening rules with critical state of dynamic recovery, part 1: formulations and basic features for ratcheting behavior," *Int. J. Plasticity*, **9**, No. 3, 375–390 (1993).
24. V. V. Novozhilov, "Nonproportional loading and prospects of the phenomenological approach to the study of microstresses," *Prikl. Matem. Mekh.*, **28**, No. 3, 393–400 (1964).
25. J.-L. Chaboche, K. Dang-Van, and G. Cordier, "Modelization of the strain memory effect on the cyclic hardening of 316 stainless steel," in: Proc. of the 5th Int. Conf. on SMiRT, Div L., Paper No. L. 11/3, Berlin (1979).
26. A. A. Ilyushin, *Continuum Mechanics* [in Russian], Publishing House of Moscow State University, Moscow (1990).